ACS OMEGA

Article

http://pubs.acs.org/journal/acsodf

Synergistically Enhanced Electrocatalytic Performance of an N-Doped Graphene Quantum Dot-Decorated 3D MoS_2−Graphene Nanohybrid for Oxygen Reduction Reaction

Ramalingam Vinoth,[†] Indrajit M. Patil,[†] Alagarsamy Pandikumar,[†] Bhalchandra A. Kakade,[†] Nay Ming Huang,[‡] Dionysiou D. Dionysios,[§] and Bernaurdshaw Neppolian*[,†]

[†]SRM Research Institute, SRM University, Kattankulathur, Kancheepuram 603203, Tamil Nadu, India

[‡]Low Dimensional Materials Research Centre, Department of Physics, Faculty of Science, University of Malaya, 50603 Kuala Lumpur, Malaysia

[§]Environmental Engineering and Science Program, Department of Biomedical, Chemical and Environmental Engineering, University of Cincinnati, Cincinnati, Ohio 45221-0012, United States

Supporting Information

ABSTRACT: Nitrogen-doped graphene quantum dots (N-GQDs) were decorated on a three-dimensional (3D) MoS_2−reduced graphene oxide (rGO) framework via a facile hydrothermal method. The distribution of N-GQDs on the 3D MoS_2−rGO framework was confirmed using X-ray photoelectron spectroscopy, energy dispersive X-ray elemental mapping, and high-resolution transmission electron microscopy techniques. The resultant 3D nanohybrid was successfully demonstrated as an efficient electrocatalyst toward the oxygen reduction reaction (ORR) under alkaline conditions. The chemical interaction between the electroactive N-GQDs and MoS_2−rGO and the increased surface area and pore size of the N-GQDs/MoS_2−rGO nanohybrid synergistically improved the ORR onset potential to +0.81 V vs reversible hydrogen electrode (RHE). Moreover, the N-GQDs/MoS_2−rGO nanohybrid showed better ORR stability for up to 3000 cycles with negligible deviation in the half-wave potential ($E_{1/2}$). Most importantly, the N-GQDs/MoS_2−rGO nanohybrid exhibited a superior methanol tolerance ability even under a high concentration of methanol (3.0 M) in alkaline medium. Hence, the development of a low-cost metal-free graphene quantum dot-based 3D nanohybrid with high methanol tolerance may open up a novel strategy to design selective cathode electrocatalysts for direct methanol fuel cell applications.

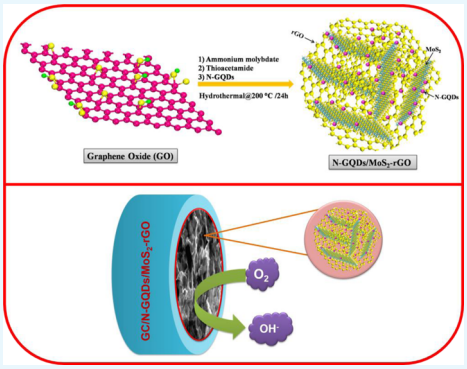

1. INTRODUCTION

Zero-dimensional (0D) graphene quantum dots (GQDs) with tunable electrical and optical properties have been considered to be impressive candidates for diverse applications including solar cells, light-emitting diodes, photocatalysts, biomedical imaging, capacitors, batteries, sensors, and fuel cells.[1−8] Recently, several advancements have been made in both theoretical and experimental studies to explore the intrinsic properties of various heteroatom-doped GQDs for electrocatalytic applications.[1,9] Previous reports reveal that the substitution of N atoms with GQDs could alter the electronic structure and offer more active sites for the oxygen reduction reaction (ORR) in fuel cells.[10−12] Qu et al. have synthesized N-doped GQDs (N-GQDs) with oxygen-rich functionalities, which exhibited superior electrocatalytic reactivity toward ORR.[1] Yet another report demonstrated the influence of the size of N-GQDs on ORR, and it showed that increasing the N-GQD size leads to an increase in the current density.[13] Similarly, N-GQDs were synthesized using an electrochemical method, and their size-dependent electrocatalytic activity for ORR was also evaluated.[14]

To utilize the potential properties of N-GQDs toward ORR, N-GQD-based hybrid electrocatalysts have also been developed recently.[10,15] In particular, the incorporation of N-GQDs on different carbon supports has attracted significant attention to fabricate alternative highly efficient electrocatalysts for ORR.[10,16] Among various carbon supports, graphene has been considered a promising support because of its exceptional physiochemical properties such as high specific surface area, high carrier mobility, excellent electrical conductivity, and good chemical stability.[17−24] Recently, boron- and nitrogen-doped GQDs were anchored on graphene platelets using a hydrothermal method and demonstrated to be an efficient electrocatalyst for ORR.[15] Similarly, a novel class of GQD-decorated graphene nanoribbon was prepared through a one-step reduction reaction for ORR.[25] Likewise, microwave-assisted functionalization of GQDs with the N and S codoped graphene electrocatalyst exhibited an excellent methanol tolerance

Received: September 29, 2016
Accepted: October 31, 2016
Published: November 18, 2016

DOI: 10.1021/acsomega.6b00275
ACS Omega 2016, 1, 971−980

Scheme 1. Schematic Illustration of the Synthesis of a 3D N-GQDs/MoS_2−rGO Nanohybrid

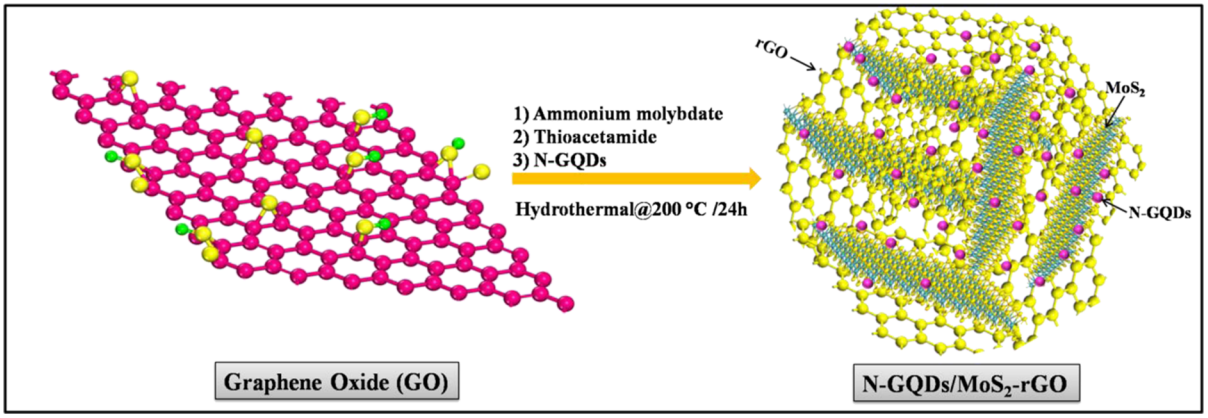

property.[26] Very recently, N-GQDs/graphene nanocomposites have been prepared using a facile self-assembly method and employed as an efficient electrocatalyst for ORR.[27] The N-rich carbon dot-incorporated graphene electrocatalyst prepared via one-pot synthesis showed a superior methanol tolerance property in an alkaline environment.[28]

In addition, two-dimensional (2D) metal chalcogenides, especially molybdenum disulfide (MoS_2), have also been demonstrated to be potential candidates for ORR because of their unique properties such as large surface area and high electrical conductivity.[29,30] However, the electrocatalytic activity of MoS_2 can be further improved by modification with different carbon supports. Recent studies have confirmed that the electrocatalytic behavior of the catalysts also depends on their morphological structure such as shape and size.[31] In particular, assembling 2D nanosheets into 3D nanostructures offers a porous structure with a large surface area and high electrical conductivity. The electrocatalytic performance of the 3D nanocomposite was higher compared with those of the catalysts with other dimensions such as 1D and 2D.[32] Recently, MoS_2−reduced graphene oxide (MoS_2−rGO) nanocomposites have been synthesized using a hydrothermal method and have been used as efficient electrocatalysts for the hydrogen evolution reaction (HER), ORR, and lithium-ion batteries.[32−35]

In the present study, we have designed N-GQD-decorated MoS_2−rGO with a 3D framework via a simple hydrothermal method as displayed in Scheme 1. This is the first report using N-GQDs along with MoS_2−rGO for ORR. The N-GQDs/MoS_2−rGO showed a 3D hierarchical framework with crumpled surfaces and edges. The resultant nanohybrid not only exhibited a better ORR onset potential of +0.81 V vs reversible hydrogen electrode (RHE) under an O_2-saturated KOH solution but also showed an excellent methanol tolerance property at a high methanol concentration. Thus, these properties make this newly prepared N-GQDs/MoS_2−rGO nanohybrid a potential selective cathode electrocatalyst for direct methanol fuel cell applications.

2. RESULTS AND DISCUSSION

UV−visible absorption spectra of N-GQDs, GO, MoS_2, MoS_2−rGO, and N-GQDs/MoS_2−rGO dispersed in deionized (DI) water are displayed in Figure 1. The N-GQDs exhibit a characteristic optical absorption peak at 348 nm.[5] This intense absorption peak is mainly attributed to the n → π^* transition that occurs in the C═O bond of N-GQDs.[4] Moreover, the N-GQDs show strong blue luminescence in the presence of UV

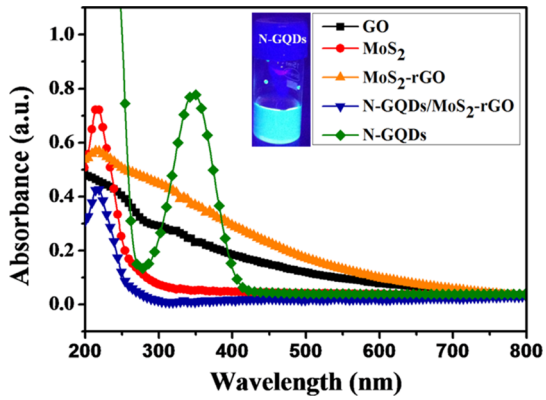

Figure 1. UV−vis absorption spectra of N-GQDs (inset: digital photograph of N-GQDs illuminated with a 365 nm, 8 W UV lamp), GO, MoS_2, MoS_2−rGO, and N-GQDs/MoS_2−rGO.

light (365 nm). This result indicates the formation of uniform sized N-GQDs. Likewise, an absorption peak noted at <300 nm for MoS_2, MoS_2−rGO, and N-GQDs/MoS_2−rGO is assigned to the excitonic features of small-sized MoS_2 nanosheets.[36] However, no absorption peak is observed for N-GQDs, which might be due to the low content of N-GQDs present in the resultant nanohybrid. On the other hand, a relatively high content of the black colored MoS_2−rGO present in the resultant N-GQDs/MoS_2−rGO can shield the photons coming into the N-GQDs.[37] This effect is commonly known as "light shielding effect".[37,38] A similar phenomenon was also observed earlier for melamine-functionalized 3D graphene sheets with CdS in photocatalytic applications.[37]

The morphological structure of the N-GQDs/MoS_2−rGO nanohybrid was examined using FE-SEM analysis. The prepared graphene oxide (GO) and MoS_2 alone showed a well-defined 2D sheetlike morphology (Figure S1). As shown in Figure 2b, the N-GQDs/MoS_2−rGO nanohybrid exhibits a typical 3D framework with wrinkled surfaces and edges. This indicates that a few layers of crumpled rGO sheets are folded with MoS_2 sheets forming a 3D nanostructure. Thus, MoS_2−rGO prepared with the 3D nanostructure can provide a high surface area for the loading of N-GQDs. Figure 2c−h gives the individual elemental mapping of the N-GQDs/MoS_2−rGO nanohybrid. Only expected elements such as Mo, S, C, O, and N are identified in the N-GQDs/MoS_2−rGO nanohybrid. The N element observed in N-GQDs/MoS_2−rGO reconfirms the existence of N-GQDs. Similarly, the EDX profile also shows

DOI: 10.1021/acsomega.6b00275
ACS Omega 2016, 1, 971−980

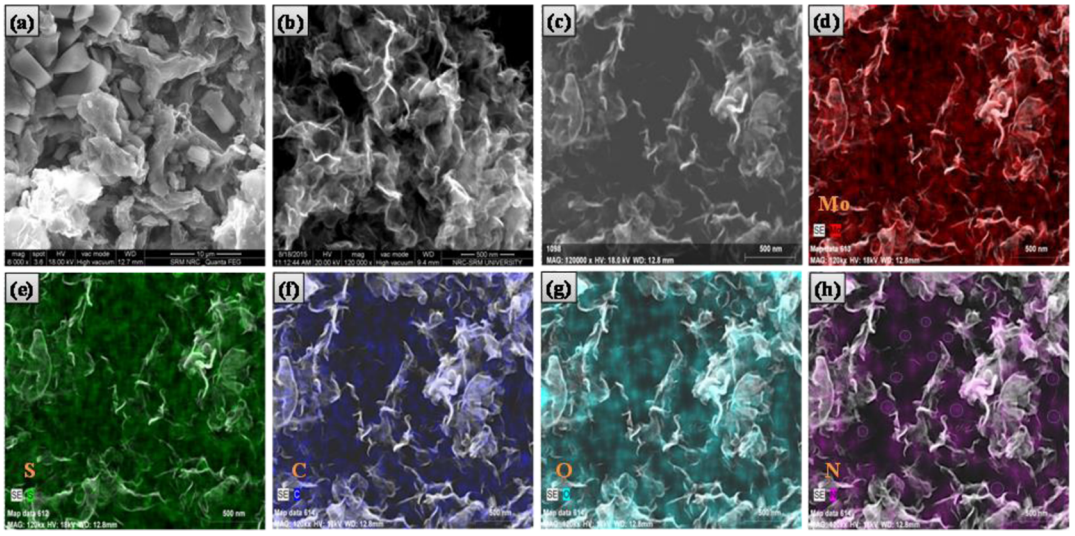

Figure 2. Field emission−scanning electron microscopy (FE-SEM) images of (a) MoS_2−rGO and (b) N-GQDs/MoS_2−rGO nanohybrid and (c) energy dispersive X-ray (EDX) mapping area of the N-GQDs/MoS_2−rGO nanohybrid and the corresponding elemental mapping of (d) Mo, (e) S, (f) C, (g) O, and (h) N elements.

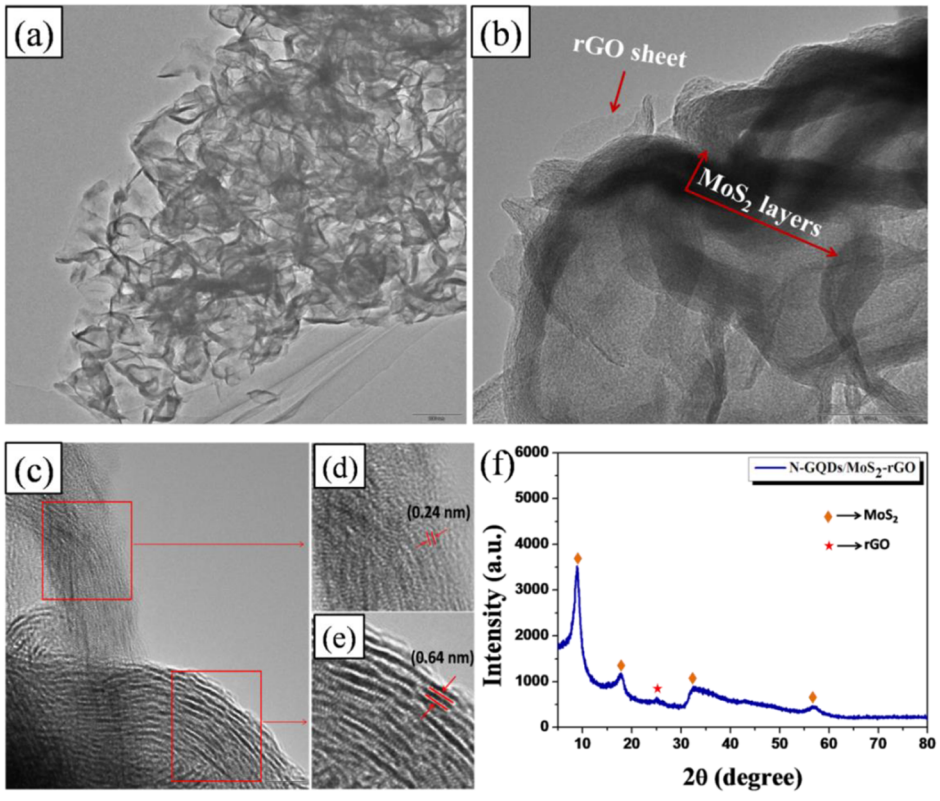

Figure 3. (a,b) Transmission electron microscopy (TEM) images of N-GQDs/MoS_2−rGO with different magnifications, (c) high-resolution TEM (HR-TEM) image of N-GQDs/MoS_2−rGO, (d,e) lattice resolved-TEM image of N-GQDs/MoS_2−rGO, and (f) X-ray diffraction (XRD) pattern of the N-GQDs/MoS_2−rGO nanohybrid.

only the Mo, S, C, O, and N elements in the synthesized nanohybrid (Figure S2).

Figure 3a,b shows the TEM images of N-GQDs/MoS_2−rGO with different magnifications. The resultant N-GQDs/MoS_2−rGO exhibits a typical 3D architecture with wrinkled surfaces or edges (Figure 3a). Thus, the obtained TEM image is similar to the FE-SEM image (Figure 2b). It is also interesting to note that the MoS_2 nanosheets and rGO sheets are intercalated with each other, which results in the formation of a 3D MoS_2−rGO nanostructure (Figure 3b). Moreover, HR-TEM studies are carried out to further confirm the incorporation of N-GQDs on the MoS_2−rGO framework. As depicted in Figure 3d,e, the marked lattice fringe values of 0.24 and 0.64 nm are assigned to the (1120) plane of the graphitic quantum dots and the (002) plane of MoS_2, respectively.[5,39] The observed (1120) crystal plane corresponding to the graphitic quantum dots clearly discloses the successful incorporation of N-GQDs on the MoS_2−rGO nanohybrid. XRD studies were performed to

DOI: 10.1021/acsomega.6b00275
ACS Omega 2016, 1, 971−980

identify the crystalline nature of the 3D hybrid. As displayed in Figure 3f, a broad diffraction peak observed at 2θ = 25° is related to the (002) crystal plane of rGO, and the corresponding *d*-spacing value is estimated to be 0.35 nm.[40] Moreover, two distinct diffraction peaks noted at the 2θ values of 32.5° and 57° are assigned to the (100) and (110) planes of MoS_2. This result clearly indicates the well-ordered atomic arrangements of MoS_2 along the basal planes.[41] More importantly, two additional peaks appeared at a low-angle region, that is, 2θ = 8.8° and 17.7°, which clearly suggests the formation of a lamellar nanostructure of MoS_2 with enlarged *d*-spacing values of 1 and 0.5 nm, respectively (JCPDS Card #: 73-1508).[42] It is worth mentioning that the oxygen functionalities of GO that intercalated between the MoS_2 sheet results in an increase in the *d*-spacing value (1 nm) of the nanohybrid compared to that of pristine MoS_2 reported elsewhere.[32,42]

Fourier transform infrared (FT-IR) spectra of GO, MoS_2−rGO, and N-GQDs/MoS_2−rGO are displayed in Figure 4. GO

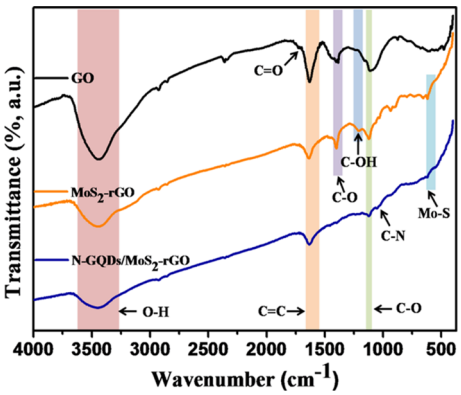

Figure 4. FT-IR spectra of GO, MoS_2−rGO, and the N-GQDs/MoS_2−rGO nanohybrid.

shows absorption peaks at 3443, 1733, 1627, 1386, 1220, and 1107 cm^{-1}, which are assigned to the O−H, C═O, C═C, C−O (carboxyl), C−OH, and C−O (alkoxy) groups, respectively.[43−45] The decrease in the peak intensity of the oxygen-rich functional groups present in MoS_2−rGO and the N-GQDs/MoS_2−rGO nanohybrid suggests the successful reduction of GO to rGO.[46] Moreover, a peak centered at 605 cm^{-1} of MoS_2−rGO and the N-GQDs/MoS_2−rGO nanohybrid corresponds to the Mo−S vibration.[47] In addition, a peak that appears at 1040 cm^{-1} of N-GQDs/MoS_2−rGO is assigned to the C−N bond present in N-GQDs.[48]

X-ray photoelectron spectroscopy (XPS) analysis was carried out to investigate the chemical nature and identify the elements present in the N-GQDs/MoS_2−rGO nanohybrid. Figure 5a shows the XPS survey scan spectrum of the N-GQDs/MoS_2−rGO nanohybrid. The predominant peaks identified at 162.5, 230.5, 284.4, 395.4, and 531.8 eV correspond to S 2p, Mo 3d, C 1s, N 1s, and O 1s core-level spectra, respectively. Two peaks identified at 228.6 and 231.8 eV for the high-resolution Mo 3d spectra are assigned to Mo $3d_{5/2}$ and Mo $3d_{3/2}$, respectively (Figure 5b).[49] The spin energy difference between the core levels of Mo $3d_{5/2}$ and Mo $3d_{3/2}$ is measured to be 3.1 eV, which indicates the Mo^{4+} oxidation state of Mo in N-GQDs/MoS_2−rGO.[50] In addition, a small peak located at 226 eV is related to S 2s.[32] In the high-resolution S 2p spectrum, S 2p and $-SO_n-$ peaks noted at 162 and 168 eV indicate the presence of sulfur species in N-GQDs/MoS_2−rGO (Figure 5c).[49,51,52] The high-resolution C 1s spectrum can be deconvoluted into four components (Figure 5d). The most intense peaks observed at 284.4 and 285.7 eV are related to the C−C/C═C and sp^3 carbon atoms or C−N bonds, respectively.[4,5] It is worth noting that the C═N bond observed at 285.1 eV confirms the presence of N-GQDs in the resultant nanohybrid.[53] Moreover, a relatively minor component occurred at 287.6 eV, which further indicates the significant reduction in oxygen-rich functionalities present in GO.[20] As shown in Figure 5e, the high-resolution N 1s spectrum is deconvoluted into four components. The main peak centered at 394.7 eV is related to Mo $3p_{3/2}$, whereas the rest of the peaks noted at 396.6, 399.8, and 401.5 eV correspond to Mo−N, pyrolic-N, and graphitic-N, respectively. Therefore, the different types of C−N bond formation observed in the N 1s spectra confirm the successful incorporation of N-GQDs on the 3D MoS_2−rGO framework.[5,50,54]

The surface area and porosity of the MoS_2−rGO and N-GQDs/MoS_2−rGO nanohybrids were investigated using Brunauer−Emmett−Teller (BET) analysis (Figure 6). As shown in Figure 6a,b, both MoS_2−rGO and N-GQDs/MoS_2−rGO nanohybrids exhibit a typical type (IV) isotherm pattern, which indicates the mesoporous nature of the catalysts.[55] The calculated BET surface areas of the MoS_2−rGO and N-GQDs/MoS_2−rGO nanohybrids are calculated to be 30.3 and 36.4 m^2/g, respectively. The pore size distributions of the MoS_2−rGO and N-GQDs/MoS_2−rGO nanohybrids are estimated using the Barrett−Joyner−Halenda (BJH) method, as shown in the inset of Figure 6a,b. The average pore sizes of the MoS_2−rGO and N-GQDs/MoS_2−rGO nanohybrids are 3.1 and 6 nm, respectively. These results suggest that the incorporation of N-GQDs on MoS_2−rGO using a hydrothermal method can enhance the surface area and the pore size of the resultant nanohybrid.[55] The increased pore size of the N-GQD-loaded MoS_2−rGO monohybrid is consistent with the FE-SEM image of the N-GQDs/MoS_2−rGO nanohybrid (Figure 2b). Moreover, the increased surface area and pore size of the N-GQD-incorporated 3D MoS_2−rGO framework can offer more catalytic active sites for effective electrochemical reactions.[56]

The electrocatalytic activity of the 3D N-GQDs/MoS_2−rGO nanohybrid-modified electrode was investigated for ORR activity in 0.1 M KOH using the three-electrode system. Figure 7a shows the CVs observed for the N-GQDs/MoS_2−rGO nanohybrid-modified electrode in N_2- and O_2-saturated 0.1 M KOH in the potential range of 0−1.2 V vs RHE. A featureless CV response occurred when the electrolyte solution was saturated with N_2. By contrast, a strong cathodic reduction peak was observed under an O_2-saturated environment, suggesting the electrocatalytic reduction of oxygen. As shown in Figure 7b, an increase in the current density with respect to the rotation speed is due to the enhanced diffusion of dissolved oxygen molecules through the porous channel of the 3D N-GQDs/MoS_2−rGO nanohybrid-modified electrode.[15] Moreover, the N-GQDs/MoS_2−rGO nanohybrid catalyst exhibits the most positive ORR onset potential of +0.81 V vs RHE and a current density of 2.56 mA/cm^2 at 1600 rpm (Figure 7b). In addition, the number of electrons transferred per oxygen molecule in the ORR process was also calculated using the Koutecky−Levich plot. A plot of J^{-1} vs $\omega^{-1/2}$ was obtained from the corresponding K−L equation (eq 1).[22]

DOI: 10.1021/acsomega.6b00275
ACS Omega 2016, 1, 971−980

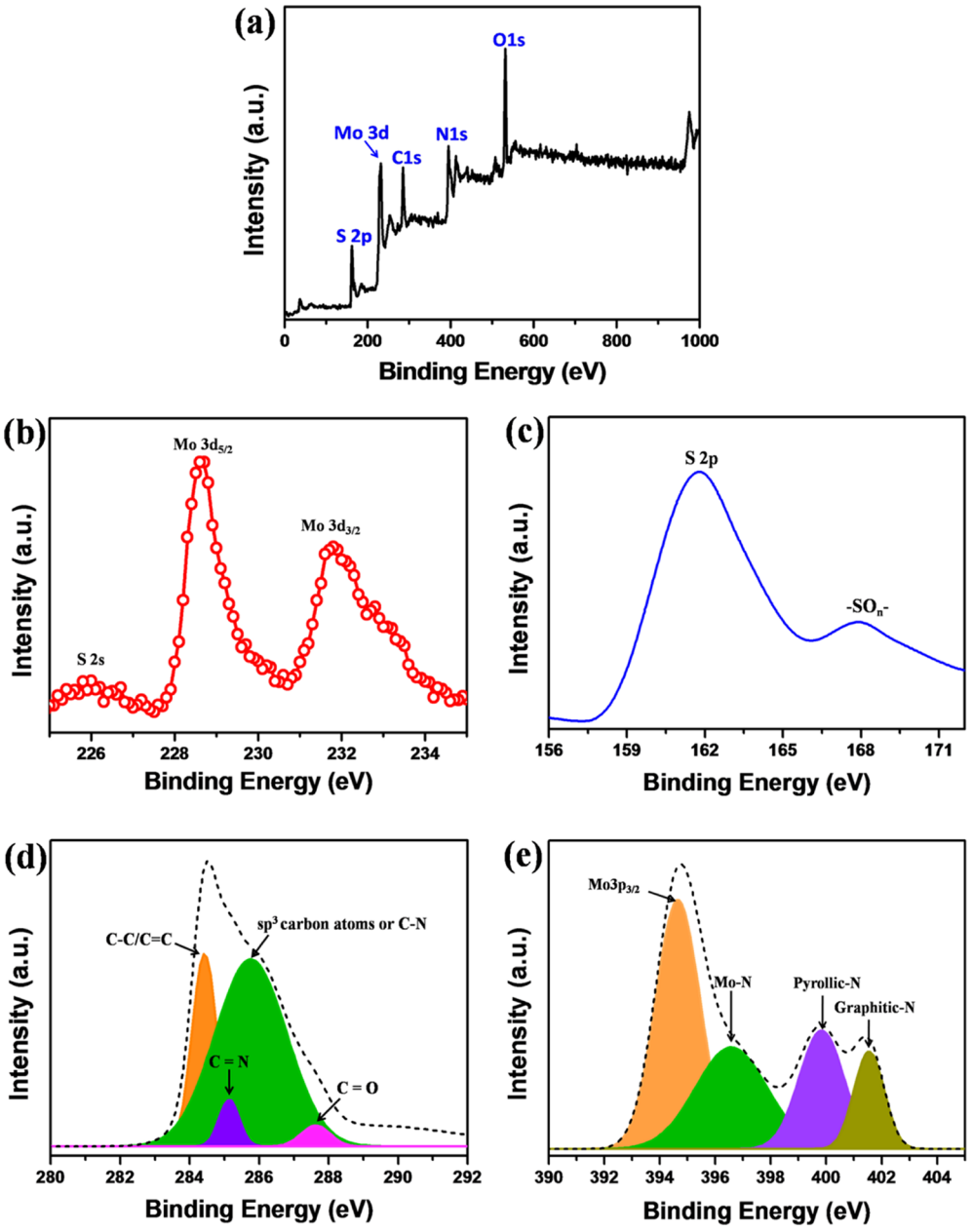

Figure 5. High-resolution XPS spectra of (a) survey scan, (b) Mo 3d, (c) S 2p, and (d) C 1s and (e) N 1s core-level spectra of N-GQDs/MoS_2−rGO.

$$\frac{1}{i} = \frac{1}{ik} + \frac{1}{id} \quad (1)$$

where i is the measured current, ik is the kinetic current, $id = B\omega^{1/2}$ is the diffusion-limiting current, B is Levich constant, and ω is the rotational speed of the electrode (eq 2). Also

$$B = 0.62nFAD_{O_2}{}^{2/3}\nu^{-1/6}C_{O_2} \quad (2)$$

where n is the number of electrons transferred per O_2 molecule, F is the Faraday constant (96 486 C mol^{-1}), A is the geometric area of the working electrode, D_{O_2} is the diffusion coefficient of the O_2 molecule (1.9×10^{-5} cm^2 s^{-1}) in 0.1 M KOH, ν is the kinematic viscosity of the electrolyte (1.9×10^{-5} cm^2 s^{-1}), and C_{O_2} is the concentration of the O_2 molecule (1.2×10^{-6} mol L^{-1}).[22,57]

Figure 7c shows the linear fitting, and the average number of electrons transferred (n) for N-GQDs/MoS_2−rGO is calculated to be about two with different potential regions, indicating the typical two-electron transfer process. The number of electrons (n) transferred in the N-GQDs/MoS_2−rGO nanohybrid can be obtained using a well-known procedure based on the RRDE assembly using the percentage of peroxide formation. As shown in Figure 7d, RRDE measurements are taken to deduce n, which is found to be between 3.2 and 3.8 in the potential region of 0.8−0 V vs RHE. On the other hand, the Koutecky−Levich approach suggests a two-electron transfer process for the N-GQDs/MoS_2−rGO nanohybrid, indicating two different electron transfer mechanisms for ORR in the present case.

The comparative LSV curves of MoS_2−rGO, N-GQDs/rGO, N-GQDs/MoS_2, and N-GQDs/MoS_2−rGO at the rotation

DOI: 10.1021/acsomega.6b00275
ACS Omega 2016, 1, 971−980

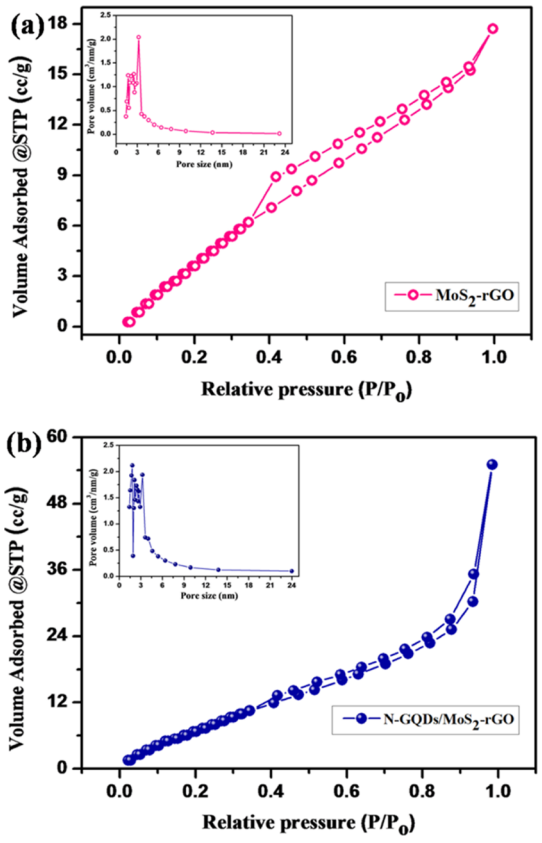

Figure 6. Nitrogen adsorption−desorption isotherms of (a) the MoS_2−rGO nanohybrid and (b) the N-GQDs/MoS_2−rGO nanohybrid and their respective pore size distributions (insets).

speed of 1600 rpm are depicted in Figure 8a. Interestingly, the N-GQDs/MoS_2−rGO nanohybrid exhibits an excellent ORR activity with the positive onset potential of +0.81 V along with the current density of 2.56 mA/cm^2. On the basis of electrochemical results and chemical nature/functionalities of the N-GQDs and MoS_2−rGO, the following explanation can be provided. In the present work, N-GQDs play a crucial role toward ORR. Electrochemically active sites on N-GQDs in conjunction with the network of MoS_2−rGO furnish improved sites for oxygen adsorption and its conversion. This effect is also clearly seen in Figure 8a, where a positive shift in the onset potential, an improved mixed diffusion and kinetic current and diffusion-controlled region is achieved. Thus, a synergistic effect between N-GQDs and MoS_2−rGO plays an important role in electrochemical activity. In addition, a larger surface area and pore size in the case of nanohybrid structures (Figure 6) can offer better catalytic active sites on the N-GQDs/MoS_2−rGO nanohybrid for effective electrochemical reactions. Moreover, a few recent reports also suggest a synergistic effect in the 3D MoS_2−rGO nanocomposite toward various catalytic processes.[49,53] The LSV curves of MoS_2−rGO-, N-GQDs/rGO-, and N-GQDs/MoS_2-modified electrodes with different rotation speeds ranging from 400 to 2500 rpm are displayed in Figure 8b−d. As shown in Figure 8a−d, LSVs of all nanocomposites show two components, one at 0.1 V and another at 0.5 V. These two components are mainly due to a two-step ORR process. The comparison of electrocatalytic performance of some carbonaceous-based electrocatalysts for the ORR process is summarized in Table S1.

The stability of the N-GQDs/MoS_2−rGO nanohybrid was evaluated for up to 3000 continuous cycles between −0.5 and

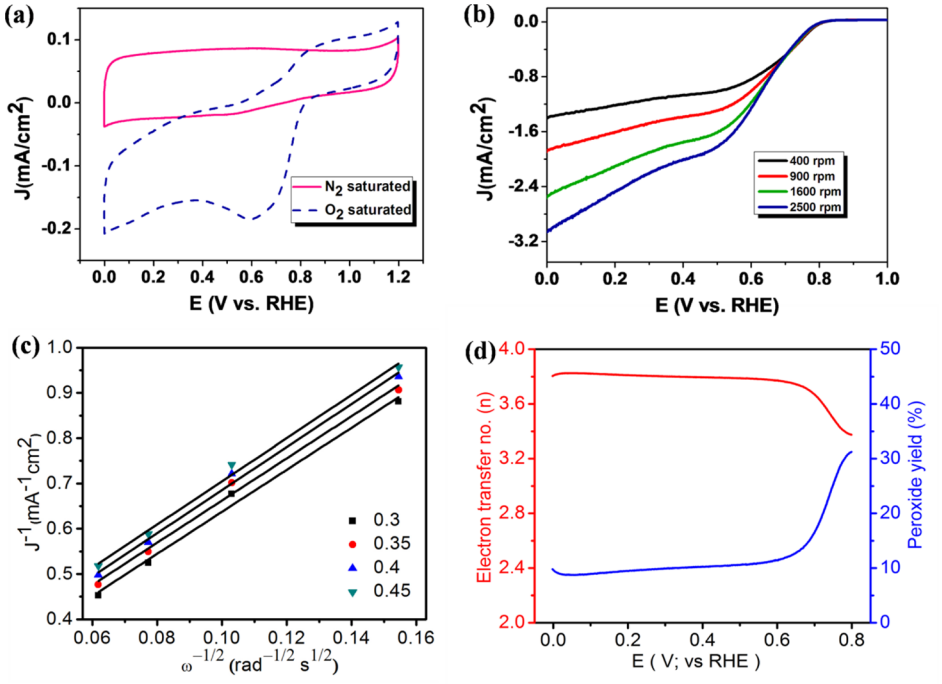

Figure 7. (a) Cyclic voltammograms (CVs) obtained for the 3D N-GQDs/MoS_2−rGO nanohybrid-modified electrode dipped into a N_2- and O_2-saturated 0.1 M KOH solution at a scan rate of 20 mV/s, (b) linear sweep voltammogram (LSV) obtained for the 3D N-GQDs/MoS_2−rGO nanohybrid-modified electrode at a scan rate of 10 mV/s with different rotation speeds ranging from 400 to 2500 rpm, (c) Koutecky−Levich (K−L) plot for the 3D N-GQDs/MoS_2−rGO-modified electrode with respect to various potentials, and (d) electron transfer number and peroxide yield for the 3D N-GQDs/MoS_2−rGO nanohybrid at the whole potential range obtained from the rotating ring disc electrode (RRDE) voltammogram, as displayed in Figure S3.

DOI: 10.1021/acsomega.6b00275
ACS Omega 2016, 1, 971−980

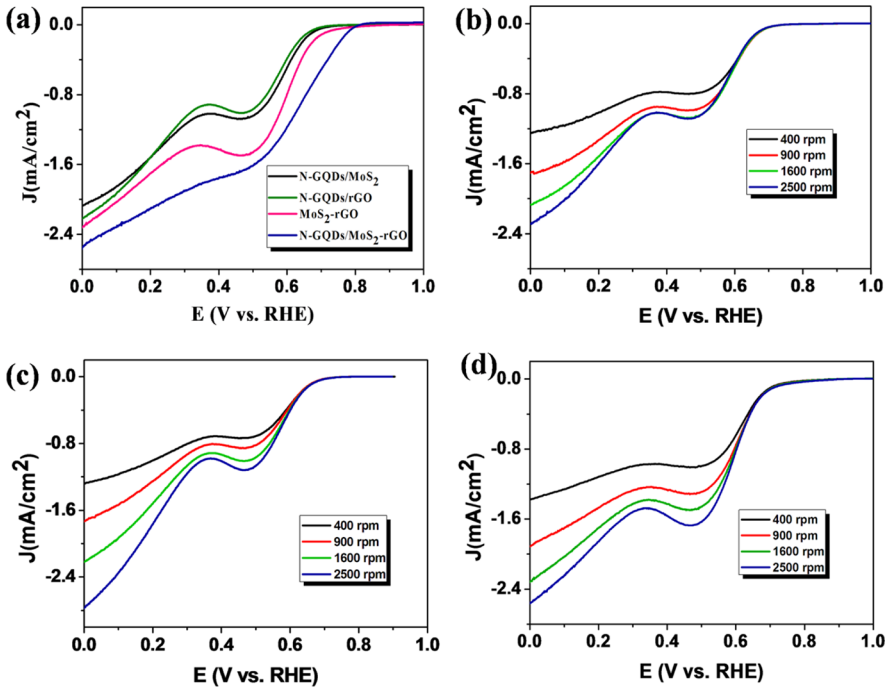

Figure 8. (a) Comparative LSV curves of N-GQDs/MoS_2-, N-GQDs/rGO-, MOS_2−rGO-, and N-GQDs/MoS_2−rGO-modified electrodes in the presence of O_2-saturated 0.1 M KOH at 1600 rpm with a scan rate of 10 mV/s, LSV obtained for (b) N-GQDs/MoS_2-, (c) N-GQDs/rGO-, and (d) MoS_2−rGO electrocatalyst-modified electrode in the presence of O_2-saturated 0.1 M KOH solution at various rotation speeds in the range of 400−2500 rpm.

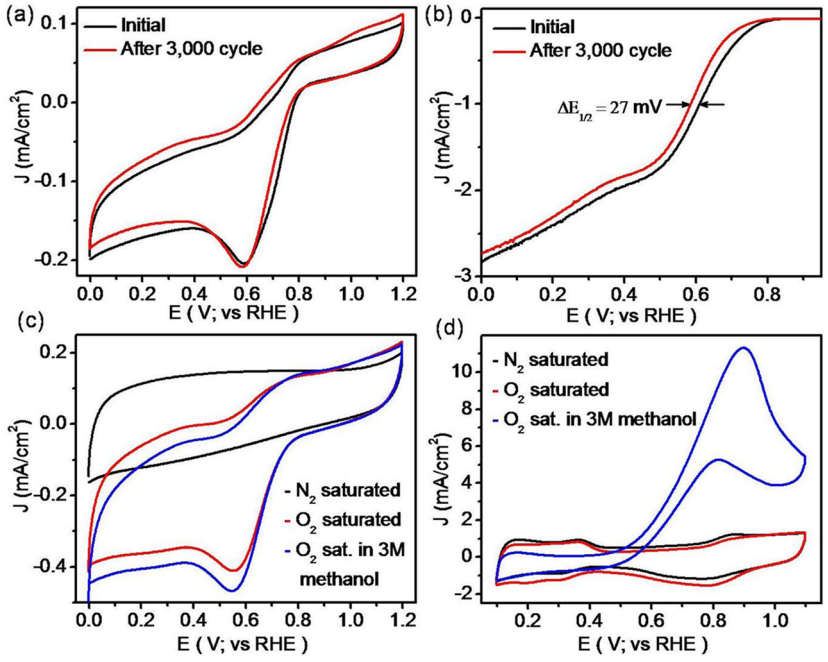

Figure 9. (a) CVs of the N-GQDs/MoS_2−rGO nanohybrid before and after 3000 cycles with a scan rate of 20 mV/s in the O_2-saturated 0.1 M KOH solution and (b) ORR polarization curves of the N-GQDs/MoS_2−rGO nanohybrid before and after 3000 cycles with a scan rate of 10 mV/s and rotation rate of 1600 rpm in the O_2-saturated 0.1 KOH solution. Comparative CVs of (c) N-GQDs/MoS_2−rGO and (d) commercial Pt/C catalyst in the presence and absence of 3 M methanol, with a sweep rate of 100 mV/s in 0.1 M KOH.

−0.1 V (vs Ag/AgCl), at a scan rate of 20 mV/s in the O_2-saturated 0.1 M KOH solution. The recorded comparative CVs and LSVs before and after the cycling tests are shown in Figure 9a,b, respectively. Importantly, the N-GQDs/MoS_2−rGO nanohybrid shows no obvious change in its CV curve after 3000 cycles (Figure 9a). In addition, the N-GQDs/MoS_2−rGO nanohybrid exhibits only a 27 mV deviation in the half-wave potential ($E_{1/2}$) for up to 3000 cycles (Figure 9b). Thus, the observed results clearly reveal better stability of the N-GQDs/MoS_2−rGO nanohybrid under alkaline conditions.

To determine the methanol tolerance ability of the resultant nanohybrid, ORR was performed at a high concentration of

DOI: 10.1021/acsomega.6b00275
ACS Omega 2016, 1, 971−980

methanol (3.0 M) in 0.1 M KOH solution and compared with commercial Pt/C (20 wt %) under similar experimental conditions.[1,58] Figure 9c,d displays the electrocatalytic activity of the N-GQDs/MoS_2−rGO nanohybrid and Pt/C in the presence and absence of methanol. As shown in Figure 9c, the N-GQDs/MoS_2−rGO catalyst exhibits almost similar voltammograms with a strong cathodic peak even at a higher concentration of methanol (3.0 M), suggesting the excellent methanol tolerance property of the N-GQDs/MoS_2−rGO nanohybrid. By contrast, Pt/C shows a substantial oxidation peak in the presence of methanol (3.0 M) under identical experimental conditions (Figure 9d). Thus, the N-GQDs/MoS_2−rGO nanohybrid with selective electrocatalytic property toward ORR could be used to replace commercial Pt/C as a cathode catalyst in a direct methanol fuel cell.

Scheme 2 represents the schematic illustration of the ORR process on the N-GQDs/MoS_2−rGO nanohybrid-modified electrode. The 3D architecture of N-GQDs/MoS_2−rGO with a highly porous structure provides more catalytic active sites to adsorb oxygen molecules. Thus, resulting in the better oxygen adsorption of the nanohybrid and the synergistic role of N-GQDs and MoS_2−rGO enhanced the ORR activity.

Scheme 2. Schematic Representation of ORR on the N-GQDs/MoS_2−rGO Nanohybrid-Modified Electrode

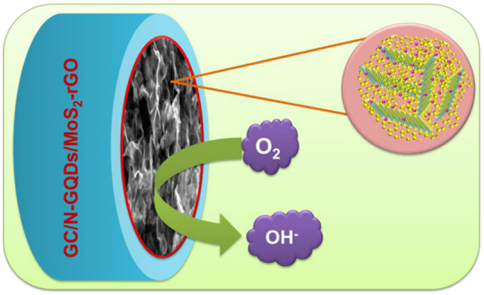

3. CONCLUSIONS

A 3D N-GQDs/MoS_2−rGO nanohybrid was developed and employed as an efficient electrocatalyst for ORR under an alkaline atmosphere. The different types of C−N bonds observed in the N 1s spectra confirmed the existence of N-GQDs on the N-GQDs/MoS_2−rGO nanohybrid. Moreover, incorporation of N-GQDs on MoS_2−rGO using the hydrothermal method increased the surface area and the pore size of the resultant nanohybrid. N-GQDs combined with MoS_2−rGO synergistically enhanced the ORR performance, with a maximum positive onset potential of +0.81 V versus RHE. The resultant N-GQDs/MoS_2−rGO showed better stability and an outstanding methanol tolerance property at a high concentration of methanol (3.0 M) to resist the methanol crossover effects in direct methanol fuel cells.

4. EXPERIMENTAL DETAILS

4.1. Chemicals. Graphite powder (synthetic, conducting grade, 325 mesh, 99.99%) was procured from Alfa Aesar. Ammonium molybdate, thioacetamide, citric acid, and ethylenediamine were purchased from SRL Chemicals, India. All chemicals were used without further purification.

4.2. Synthesis of GO and N-GQDs. GO was synthesized from graphite flakes using the modified Hummers' method.[59] N-GQDs were prepared using a hydrothermal method.[5] In brief, 1.68 g of citric acid and 1.44 g of ethylenediamine were mixed in 40 mL of DI water and stirred to get a clear solution. Then, the mixture was transferred into a 50 mL Teflon-lined autoclave and heated at 160 °C for 4 h. Finally, the product was collected through centrifugation and redispersed in DI water.

4.3. Synthesis of the N-GQD-Decorated 3D MoS_2−rGO Nanohybrid. The 3D N-GQDs/MoS_2−rGO nanohybrid was prepared via a simple hydrothermal method (Scheme 1). In brief, 40 mg of GO was first dispersed in 40 mL of DI water and ultrasonicated (Bath-type ultrasonicator, Labman-LMUC-25, operating frequency is 40 kHz, and the rated output power is 600 W) for 30 min to make a homogeneous dispersion. Subsequently, 106 mg of ammonium molybdate and 240 mg of thioacedamide were dissolved in 40 mL of DI water separately and stirred for 30 min. Then, the predispersed GO solution was slowly added into the above reaction mixture under constant stirring. Followed by GO addition, 1 mL of the as-synthesized N-GQDs predispersed in DI water was injected into the above reaction mixture and stirred for 10 min. Afterward, the solution was placed in a 100 mL Teflon-lined stainless steel autoclave and heated at 200 °C for 24 h in an electric hot air oven. Finally, the obtained fine black solids were washed several times with DI water followed by washing with ethanol and dried at 80 °C overnight. The resultant product was named the N-GQDs/MoS_2−rGO nanohybrid. For comparison, MoS_2−rGO, N-GQDs/MoS_2, and N-GQDs/rGO were also synthesized under identical experimental conditions.

4.4. Characterization Studies. UV−vis absorption spectra were obtained using a Specord 200 plus spectrophotometer (Analytikjena, Germany). XRD analysis was performed using a PANaltical X'pert powder diffractometer using Cu Kα radiation (λ = 1.5418 Å). The surface morphology, elemental mapping, and analysis were examined by FE-SEM and EDX using an FEI Quanta FEG 200 high-resolution scanning electron microscope. HR-TEM images were recorded using a JEOL JEM 2100F transmission electron microscope. XPS measurements were obtained using a Shimadzu ESCA 3100, and the FT-IR spectra were recorded using an FTIR spectrophotometer (Agilent, Cary 660, USA). The surface area and the pore size of the resultant electrocatalyst were analyzed using a Quantachrome Nova-1000 surface analyzer.

4.5. Fabrication of a Modified Electrode and Electrochemical Studies. The N-GQDs/MoS_2−rGO nanohybrid-modified glassy carbon (GC) electrode was fabricated as follows. Before the electrode modification, the GC electrode was polished with alumina slurry (0.05 micron). The N-GQDs/MoS_2−rGO ink was prepared by homogeneously dispersing 5 mg of sample into 3 mL of 24% of isopropyl alcohol with 25 μL Nafion (5 wt%). Then, this mixture was ultrasonicated for 30 min under ice-cold conditions. Finally, 4 μL of the as-prepared ink was carefully dropped on the well-cleaned GC electrode surface and dried under an ethanol atmosphere. Before the electrochemical measurement, the electrolyte solution was purged with ultrapure N_2 or O_2 gas for up to 30 min to achieve the saturation condition.

Electrochemical measurements were performed using a CHI760E bipotentiostat workstation (CH Instruments, Inc., USA) with a typical three-electrode configuration using Pt wire and Ag/AgCl (saturated in KCl) and modified GC (geometric area 0.0707 cm^2) as the counter, reference, and working electrodes, respectively. An aqueous solution of 0.1 M KOH was used as the electrolyte throughout all electrochemical measurements. Finally, all measurements were converted from

DOI: 10.1021/acsomega.6b00275
ACS Omega 2016, 1, 971−980

Ag/AgCl to RHE ($E_{RHE} = E_{Ag/AgCl} + 0.998$ V).[22] The stability of the N-GQDs/MoS_2−rGO nanohybrid was evaluated up to 3000 cycles with a scan rate of 10 mV/s and a rotation speed of 1600 rpm in 0.1 KOH solution. In the case of RRDE, the catalyst inks and electrodes were prepared in the same manner as above for RDE measurements, with the only difference in the amount of catalyst inks loaded on the disc electrode. In brief, 10 μL of catalyst inks was carefully dropped on the disc electrode (diameter of 4 mm). In the RRDE measurements, the electrode was scanned with a sweep rate of 10 mV/s, and the ring potential was fixed at 0.5 V vs Ag/AgCl. Equations 3 and 4 were used to calculate the peroxide (% HO_2^-) yield and the number of electrons transferred.

$$(\%\ HO_2^-) = 200 \times \frac{I_r/N}{I_D + I_r/N} \quad (3)$$

$$n = 4 \times \frac{I_D}{I_D + I_r/N} \quad (4)$$

where I_D is the disc current, I_r is the ring current, and $N = 0.38$ is the current collection efficiency of the Pt ring.

■ ASSOCIATED CONTENT

Supporting Information

The Supporting Information is available free of charge on the ACS Publications website at DOI: 10.1021/acsomega.6b00275.

FE-SEM image of GO and MoS_2, EDX spectra of N-GQDs/MoS_2−rGO, RRDE voltammogram, LSV curve of the commercial Pt/C and N-GQDs/MoS_2−rGO nanohybrid and comparison table for the carbaneous-based electrocatalysts for ORR studies (PDF)

■ AUTHOR INFORMATION

Corresponding Author

*E-mail: neppolian.b@res.srmuniv.ac.in. Phone: +91-44-2741-7916. Fax: +91-44-2745-6702 (B.N.).

Notes

The authors declare no competing financial interest.

■ ACKNOWLEDGMENTS

The authors gratefully acknowledge the Department of Science and Technology−Science and Engineering Research Board (DST-SERB), New Delhi, India (File No: EMR/2014/000645) and the Ministry of New and Renewable Energy (MNRE), New Delhi, India (File No: 103/239/2015-NT) for their financial support to carry out this research work.

■ REFERENCES

(1) Li, Y.; Zhao, Y.; Cheng, H.; Hu, Y.; Shi, G.; Dai, L.; Qu, L. Nitrogen-Doped Graphene Quantum Dots with Oxygen-Rich Functional Groups. *J. Am. Chem. Soc.* **2012**, *134*, 15−18.

(2) Yang, S.-T.; Cao, L.; Luo, P. G.; Lu, F.; Wang, X.; Wang, H.; Meziani, M. J.; Liu, Y.; Qi, G.; Sun, Y.-P. Carbon Dots for Optical Imaging in Vivo. *J. Am. Chem. Soc.* **2009**, *131*, 11308−11309.

(3) Baker, S. N.; Baker, G. A. Luminescent Carbon Nanodots: Emergent Nanolights. *Angew. Chem., Int. Ed.* **2010**, *49*, 6726−6744.

(4) Qu, D.; Zheng, M.; Li, J.; Xie, Z.; Sun, Z. Tailoring Color Emissions from N-Doped Graphene Quantum Dots for Bioimaging Applications. *Light: Sci. Appl.* **2015**, *4*, No. e364.

(5) Qu, D.; Zheng, M.; Zhang, L.; Zhao, H.; Xie, Z.; Jing, X.; Haddad, R. E.; Fan, H.; Sun, Z. Formation Mechanism and Optimization of Highly Luminescent N-Doped Graphene Quantum Dots. *Sci. Rep.* **2014**, *4*, 5294.

(6) Liu, W.-W.; Feng, Y.-Q.; Yan, X.-B.; Chen, J.-T.; Xue, Q.-J. Superior Micro-Supercapacitors Based on Graphene Quantum Dots. *Adv. Funct. Mater.* **2013**, *23*, 4111−4122.

(7) Chao, D.; Zhu, C.; Xia, X.; Liu, J.; Zhang, X.; Wang, J.; Liang, P.; Lin, J.; Zhang, H.; Shen, Z. X.; Fan, H. J. Graphene Quantum Dots Coated VO_2 Arrays for Highly Durable Electrodes for Li and Na ion Batteries. *Nano Lett.* **2015**, *15*, 565−573.

(8) Wang, F.; Gu, Z.; Lei, W.; Wang, W.; Xia, X.; Hao, Q. Graphene Quantum Dots as a Fluorescent Sensing Platform for Highly Efficient Detection of Copper(II) ions. *Sens. Actuators, B* **2014**, *190*, 516−522.

(9) Saidi, W. A. Oxygen Reduction Electrocatalysis using N-Doped Graphene Quantum-Dots. *J. Phys. Chem. Lett.* **2013**, *4*, 4160−4165.

(10) Zhou, X.; Tian, Z.; Li, J.; Ruan, H.; Ma, Y.; Yang, Z.; Qu, Y. Synergistically Enhanced Activity of Graphene Quantum Dot/Multi-Walled Carbon Nanotube Composites as Metal-Free Catalysts for Oxygen Reduction Reaction. *Nanoscale* **2014**, *6*, 2603−2607.

(11) Kundu, S.; Yadav, R. M.; Narayanan, T. N.; Shelke, M. V.; Vajtai, R.; Ajayan, P. M.; Pillai, V. K. Synthesis of N, F and S Co-Doped Graphene Quantum Dots. *Nanoscale* **2015**, *7*, 11515−11519.

(12) Tang, L.; Ji, R.; Li, X.; Teng, K. S.; Lau, S. P. Energy-Level Structure of Nitrogen-Doped Graphene Quantum Dots. *J. Mater. Chem. C* **2013**, *1*, 4908−4915.

(13) Li, Q.; Zhang, S.; Dai, L.; Li, L.-S. Nitrogen-Doped Colloidal Graphene Quantum Dots and their Size-Dependent Electrocatalytic Activity for the Oxygen Reduction Reaction. *J. Am. Chem. Soc.* **2012**, *134*, 18932−18935.

(14) Shinde, D. B.; Vishal, M. V.; Kurungot, S.; Pillai, V. K. Electrochemical Preparation of Nitrogen-Doped Graphene Quantum Dots and their Size-Dependent Electrocatalytic Activity for Oxygen Reduction. *Bull. Mater. Sci.* **2015**, *38*, 435−442.

(15) Fei, H.; Ye, R.; Ye, G.; Gong, Y.; Peng, Z.; Fan, X.; Samuel, E. L. G.; Ajayan, P. M.; Tour, J. M. Boron- and Nitrogen-Doped Graphene Quantum Dots/Graphene Hybrid Nanoplatelets as Efficient Electrocatalysts for Oxygen Reduction. *ACS Nano* **2014**, *8*, 10837−10843.

(16) Zhang, B.; Xiao, C.; Xiang, Y.; Dong, B.; Ding, S.; Tang, Y. Nitrogen-Doped Graphene Quantum Dots Anchored on Thermally Reduced Graphene Oxide as an Electrocatalyst for the Oxygen Reduction Reaction. *ChemElectroChem* **2016**, *3*, 864−870.

(17) Kamat, P. V. Graphene-Based Nanoassemblies for Energy Conversion. *J. Phys. Chem. Lett.* **2011**, *2*, 242−251.

(18) Seger, B.; Kamat, P. V. Electrocatalytically Active Graphene-Platinum Nanocomposites. Role of 2-D Carbon Support in PEM Fuel Cells. *J. Phys. Chem. C* **2009**, *113*, 7990−7995.

(19) Vinodgopal, K.; Neppolian, B.; Lightcap, I. V.; Grieser, F.; Ashokkumar, M.; Kamat, P. V. Sonolytic Design of Graphene−Au Nanocomposites. Simultaneous and Sequential Reduction of Graphene Oxide and Au(III). *J. Phys. Chem. Lett.* **2010**, *1*, 1987−1993.

(20) Babu, S. G.; Vinoth, R.; Kumar, D. P.; Shankar, M. V.; Chou, H.-L.; Vinodgopal, K.; Neppolian, B. Influence of Electron Storing, Transferring and Shuttling Assets of Reduced Graphene Oxide at the Interfacial Copper Doped TiO_2 p−n Heterojunction for Increased Hydrogen Production. *Nanoscale* **2015**, *7*, 7849−7857.

(21) Babu, S. G.; Vinoth, R.; Neppolian, B.; Dionysiou, D. D.; Ashokkumar, M. Diffused Sunlight Driven Highly Synergistic Pathway for Complete Mineralization of Organic Contaminants using Reduced Graphene Oxide Supported Photocatalyst. *J. Hazard. Mater.* **2015**, *291*, 83−92.

(22) Patil, I. M.; Lokanathan, M.; Kakade, B. Three Dimensional Nanocomposite of Reduced Graphene Oxide and Hexagonal Boron Nitride as an Efficient Metal-Free Catalyst for Oxygen Electroreduction. *J. Mater. Chem. A* **2016**, *4*, 4506−4515.

(23) Maliyekkal, S. M.; Sreeprasad, T. S.; Krishnan, D.; Kouser, S.; Mishra, A. K.; Waghmare, U. V.; Pradeep, T. Graphene: A Reusable Substrate for Unprecedented Adsorption of Pesticides. *Small* **2013**, *9*, 273−283.

(24) Koushik, D.; Gupta, S. S.; Maliyekkal, S. M.; Pradeep, T. Rapid Dehalogenation of Pesticides and Organics at the Interface of Reduced Graphene Oxide−Silver Nanocomposite. *J. Hazard. Mater.* **2016**, *308*, 192−198.

DOI: 10.1021/acsomega.6b00275
ACS Omega 2016, 1, 971−980

(25) Jin, H.; Huang, H.; He, Y.; Feng, X.; Wang, S.; Dai, L.; Wang, J. Graphene Quantum Dots Supported by Graphene Nanoribbons with Ultrahigh Electrocatalytic Performance for Oxygen Reduction. *J. Am. Chem. Soc.* **2015**, *137*, 7588−7591.
(26) Luo, Z.; Yang, D.; Qi, G.; Shang, J.; Yang, H.; Wang, Y.; Yuwen, L.; Yu, T.; Huang, W.; Wang, L. Microwave-Assisted Solvothermal Preparation of Nitrogen and Sulfur Co-Doped Reduced Graphene Oxide and Graphene Quantum Dots Hybrids for Highly Efficient Oxygen Reduction. *J. Mater. Chem. A* **2014**, *2*, 20605−20611.
(27) Fan, M.; Zhu, C.; Yang, J.; Sun, D. Facile Self-Assembly N-Doped Graphene Quantum Dots/Graphene for Oxygen Reduction Reaction. *Electrochim. Acta* **2016**, *216*, 102−109.
(28) Niu, W.-J.; Zhu, R.-H.; Zeng, H.-B.; Cosnier, S.; Zhang, X.-J.; Shan, D. One-Pot Synthesis of Nitrogen-Rich Carbon Dots Decorated Graphene Oxide as Metal-Free Electrocatalyst for Oxygen Reduction Reaction. *Carbon* **2016**, *109*, 402−410.
(29) Kibsgaard, J.; Chen, Z.; Reinecke, B. N.; Jaramillo, T. F. Engineering the Surface Structure of MoS_2 to Preferentially Expose Active Edge Sites for Electrocatalysis. *Nat. Mater.* **2012**, *11*, 963−969.
(30) Wang, T.; Gao, D.; Zhuo, J.; Zhu, Z.; Papakonstantinou, P.; Li, Y.; Li, M. Size-Dependent Enhancement of Electrocatalytic Oxygen-Reduction and Hydrogen-Evolution Performance of MoS_2 Particles. *Chem.—Eur. J.* **2013**, *19*, 11939−11948.
(31) Kiran, V.; Srinivasu, K.; Sampath, S. Morphology Dependent Oxygen Reduction Activity of Titanium Carbide: Bulk vs. Nanowires. *Phys. Chem. Chem. Phys.* **2013**, *15*, 8744−8751.
(32) Zhou, W.; Zhou, K.; Hou, D.; Liu, X.; Li, G.; Sang, Y.; Liu, H.; Li, L.; Chen, S. Three-Dimensional Hierarchical Frameworks Based on MoS_2 Nanosheets Self-Assembled on Graphene Oxide for Efficient Electrocatalytic Hydrogen Evolution. *ACS Appl. Mater. Interfaces* **2014**, *6*, 21534−21540.
(33) Gopalakrishnan, K.; Pramoda, K.; Maitra, U.; Mahima, U.; Shah, M. A.; Rao, C. N. R. Performance of MoS_2-Reduced Graphene Oxide Nanocomposites in Supercapacitors and in Oxygen Reduction Reaction. *Nanomater. Energy* **2015**, *4*, 9−17.
(34) Huang, G.; Chen, T.; Chen, W.; Wang, Z.; Chang, K.; Ma, L.; Huang, F.; Chen, D.; Lee, J. Y. Graphene-Like MoS_2/Graphene Composites: Cationic Surfactant-Assisted Hydrothermal Synthesis and Electrochemical Reversible Storage of Lithium. *Small* **2013**, *9*, 3693−3703.
(35) Zhao, B.; Wang, Z.; Gao, Y.; Chen, L.; Lu, M.; Jiao, Z.; Jiang, Y.; Ding, Y.; Cheng, L. Hydrothermal synthesis of layer-controlled MoS_2/graphene composite aerogels for lithium-ion battery anode materials. *Appl. Surf. Sci.* **2016**, *390*, 209−215.
(36) Gopalakrishnan, D.; Damien, D.; Shaijumon, M. M. MoS_2 Quantum Dot-Interspersed Exfoliated MoS_2 Nanosheets. *ACS Nano* **2014**, *8*, 5297−5303.
(37) Weng, B.; Xu, Y.-J. What if the Electrical Conductivity of Graphene Is Significantly Deteriorated for the Graphene−Semiconductor Composite-Based Photocatalysis? *ACS Appl. Mater. Interfaces* **2015**, *7*, 27948−27958.
(38) Yan, Y.; Sun, S.; Song, Y.; Yan, X.; Guan, W.; Liu, X.; Shi, W. Microwave-Assisted in Situ Synthesis of Reduced Graphene Oxide-$BiVO_4$ Composite Photocatalysts and their Enhanced Photocatalytic Performance for the Degradation of Ciprofloxacin. *J. Hazard. Mater.* **2013**, *250*−*251*, 106−114.
(39) Chang, K.; Mei, Z.; Wang, T.; Kang, Q.; Ouyang, S.; Ye, J. MoS_2/Graphene Cocatalyst for Efficient Photocatalytic H_2 Evolution under Visible Light Irradiation. *ACS Nano* **2014**, *8*, 7078−7087.
(40) Wei, Z.; Pan, R.; Hou, Y.; Yang, Y.; Liu, Y. Graphene-Supported Pd Catalyst for Highly Selective Hydrogenation of Resorcinol to 1, 3-Cyclohexanedione through Giant π-Conjugate Interactions. *Sci. Rep.* **2015**, *5*, 15664.
(41) Li, H.; Yu, K.; Li, C.; Tang, Z.; Guo, B.; Lei, X.; Fu, H.; Zhu, Z. Charge-Transfer Induced High Efficient Hydrogen Evolution of MoS_2/Graphene Cocatalyst. *Sci. Rep.* **2015**, *5*, 18730.
(42) Xie, J.; Zhang, J.; Li, S.; Grote, F.; Zhang, X.; Zhang, H.; Wang, R.; Lei, Y.; Pan, B.; Xie, Y. Controllable Disorder Engineering in Oxygen-Incorporated MoS_2 Ultrathin Nanosheets for Efficient Hydrogen Evolution. *J. Am. Chem. Soc.* **2013**, *135*, 17881−17888.
(43) Lin, L.; Zhang, S. Effective Solvothermal Deoxidization of Graphene Oxide using Solid Sulphur as a Reducing Agent. *J. Mater. Chem.* **2012**, *22*, 14385−14393.
(44) Vinoth, R.; Babu, S. G.; Bahnemann, D.; Neppolian, B. Nitrogen Doped Reduced Graphene Oxide Hybrid Metal Free Catalyst for Effective Reduction of 4-Nitrophenol. *Sci. Adv. Mater.* **2015**, *7*, 1443−1449.
(45) Yang, T.; Liu, L.-h.; Liu, J.-w.; Chen, M.-L.; Wang, J.-H. Cyanobacterium Metallothionein Decorated Graphene Oxide Nanosheets for Highly Selective Adsorption of Ultra-Trace Cadmium. *J. Mater. Chem.* **2012**, *22*, 21909−21916.
(46) Vinoth, R.; Karthik, P.; Muthamizhchelvan, C.; Ashokkumar, M.; Neppolian, B. Carrier Separation and Charge Transport Characteristics of Reduced Graphene Oxide Supported Visible-Light Active Photocatalysts. *Phys. Chem. Chem. Phys.* **2016**, *18*, 5179−5191.
(47) Karade, S. S.; Dubal, D. P.; Sankapal, B. R. MoS_2 Ultrathin Nanoflakes for High Performance Supercapacitors: Room Temperature Chemical Bath Deposition (CBD). *RSC Adv.* **2016**, *6*, 39159−39165.
(48) Hu, C.; Liu, Y.; Yang, Y.; Cui, J.; Huang, Z.; Wang, Y.; Yang, L.; Wang, H.; Xiao, Y.; Rong, J. One-Step Preparation of Nitrogen-Doped Graphene Quantum Dots from Oxidized Debris of Graphene Oxide. *J. Mater. Chem. B* **2013**, *1*, 39−42.
(49) Zhao, Y.; Kuai, L.; Liu, Y.; Wang, P.; Arandiyan, H.; Cao, S.; Zhang, J.; Li, F.; Wang, Q.; Geng, B.; Sun, H. Well-Constructed Single-Layer Molybdenum Disulfide Nanorose Cross-Linked by Three Dimensional-Reduced Graphene Oxide Network for Superior Water Splitting and Lithium Storage Property. *Sci. Rep.* **2015**, *5*, 8722.
(50) Liu, J.; Tang, S.; Lu, Y.; Cai, G.; Liang, S.; Wang, W.; Chen, X. Synthesis of Mo_2N Nanolayer Coated MoO_2 Hollow Nanostructures as High-Performance Anode Materials for Lithium-Ion Batteries. *Energy Environ. Sci.* **2013**, *6*, 2691−2697.
(51) Shi, Y.; Huang, J.-K.; Jin, L.; Hsu, Y.-T.; Yu, S. F.; Li, L.-J.; Yang, H. Y. Selective Decoration of Au Nanoparticles on Monolayer MoS_2 Single Crystals. *Sci. Rep.* **2013**, *3*, 1839.
(52) Tian, W.; Zhang, H.; Duan, X.; Sun, H.; Tade, M. O.; Ang, H. M.; Wang, S. Nitrogen- and Sulfur-Codoped Hierarchically Porous Carbon for Adsorptive and Oxidative Removal of Pharmaceutical Contaminants. *ACS Appl. Mater. Interfaces* **2016**, *8*, 7184−7193.
(53) Dong, H.; Liu, C.; Ye, H.; Hu, L.; Fugetsu, B.; Dai, W.; Cao, Y.; Qi, X.; Lu, H.; Zhang, X. Three-Dimensional Nitrogen-Doped Graphene Supported Molybdenum Disulfide Nanoparticles as an Advanced Catalyst for Hydrogen Evolution Reaction. *Sci. Rep.* **2015**, *5*, 17542.
(54) Zhou, W.; Hou, D.; Sang, Y.; Yao, S.; Zhou, J.; Li, G.; Li, L.; Liu, H.; Chen, S. MoO_2 Nanobelts@Nitrogen Self-Doped MoS_2 Nanosheets as Effective Electrocatalysts for Hydrogen Evolution Reaction. *J. Mater. Chem. A* **2014**, *2*, 11358−11364.
(55) Iturbe-Ek, J.; Andrade-Martínez, J.; Gómez, R.; Rodríguez-González, V. A Functional Assembly of SiO_2 Nanospheres/Graphene Oxide Composites. *Mater. Lett.* **2015**, *142*, 75−79.
(56) Lai, F.; Miao, Y.-E.; Huang, Y.; Zhang, Y.; Liu, T. Nitrogen-Doped Carbon Nanofiber/Molybdenum Disulfide Nanocomposites Derived from Bacterial Cellulose for High-Efficiency Electrocatalytic Hydrogen Evolution Reaction. *ACS Appl. Mater. Interfaces* **2016**, *8*, 3558−3566.
(57) Lai, L.; Potts, J. R.; Zhan, D.; Wang, L.; Poh, C. K.; Tang, C.; Gong, H.; Shen, Z.; Lin, J.; Ruoff, R. S. Exploration of the Active Center Structure of Nitrogen-Doped Graphene-Based Catalysts for Oxygen Reduction Reaction. *Energy Environ. Sci.* **2012**, *5*, 7936−7942.
(58) Liu, R.; Wu, D.; Feng, X.; Müllen, K. Nitrogen-Doped Ordered Mesoporous Graphitic Arrays with High Electrocatalytic Activity for Oxygen Reduction. *Angew. Chem.* **2010**, *122*, 2619−2623.
(59) Hummers, W. S.; Offeman, R. E. Preparation of Graphitic Oxide. *J. Am. Chem. Soc.* **1958**, *80*, 1339.

DOI: 10.1021/acsomega.6b00275
ACS Omega 2016, 1, 971−980